Molecular Cell

Supplemental Information

Toxicity of Eosinophil MBP Is Repressed by Intracellular Crystallization and Promoted by Extracellular Aggregation

Alice Soragni, Shida Yousefi, Christina Stoeckle, Angela B. Soriaga, Michael R. Sawaya, Evelyne Kozlowski, Inès Schmid, Susanne Radonjic-Hoesli, Sebastien Boutet, Garth J. Williams, Marc Messerschmidt, M. Marvin Seibert, Duilio Cascio, Nadia A. Zatsepin, Manfred Burghammer, Christian Riekel, Jacques-Philippe Colletier, Roland Riek, David S. Eisenberg, and Hans-Uwe Simon

SUPPLEMENTAL FIGURES

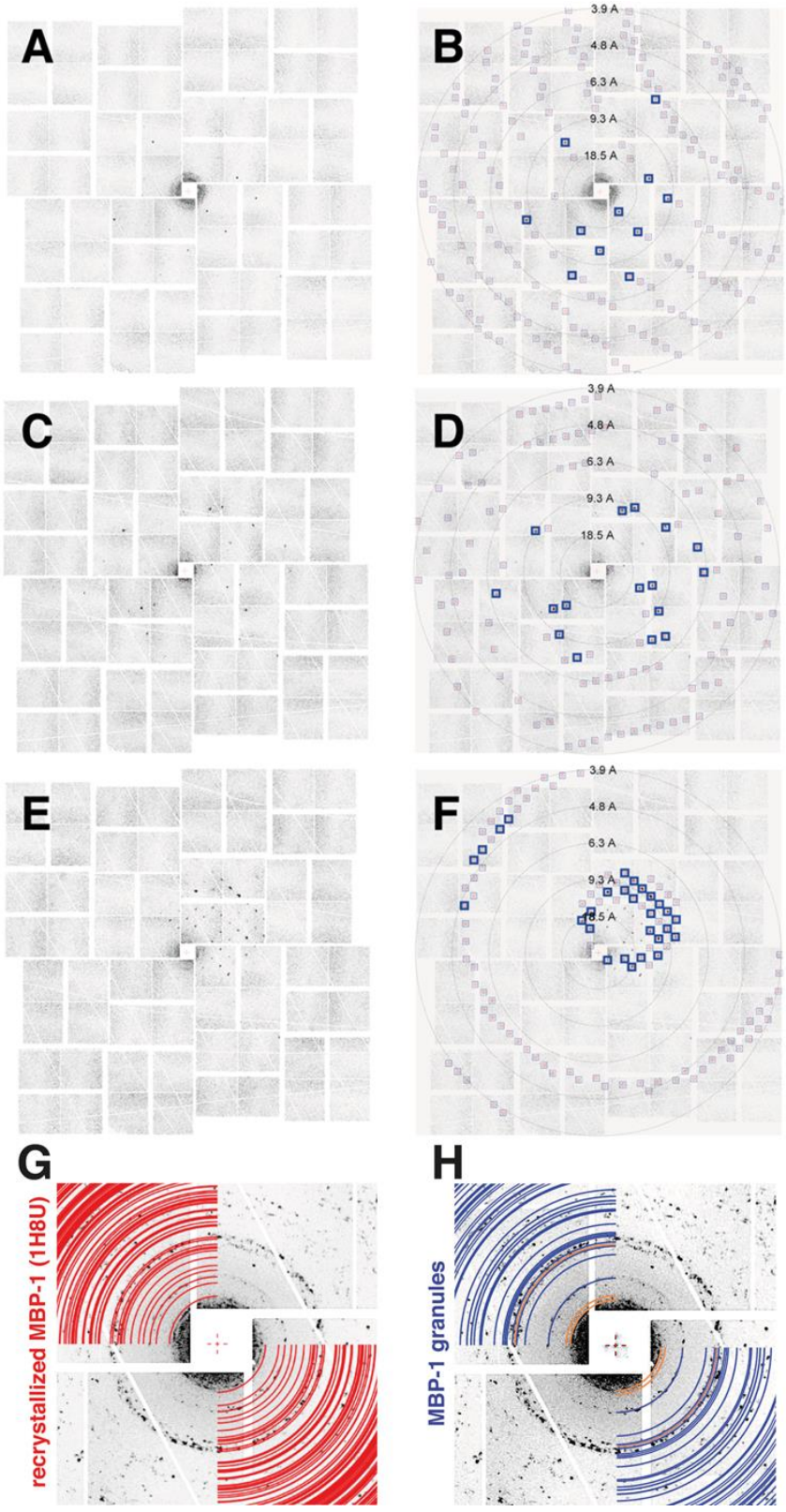

Figure S1. MBP-1 Nanocrystals Diffraction Obtained by XFEL Radiation and Comparison of Lattice Spacings of Purified and Recrystallized MBP-1 (related to Fig. 1)

(A, C, E) Diffraction patterns obtained from granule embedded MBP-1 single crystals by XFEL radiation.

(B, D, F) Diffraction patterns overlaid with predictions from the derived lattice constants. The blue boxes highlight those predicted diffraction spots which were observed experimentally. The detector is a mosaic of pixel array chips. The white lines at various angles trace the wire mask used for panel alignment, same as in Figure 1.

(G) Intragranular nanocrystals XFEL maximum projection overlaid with powder rings predicted from the recrystallized 1H8U cell. The observed diffraction from *in vivo* formed nanocrystals does not overlap with the recrystallized MBP-1, confirming substantial differences in the *in vivo* vs. *in vitro* packing.

(H) Intragranular nanocrystals XFEL maximum projection overlaid with powder rings predicted from the XFEL derived cell dimensions. The orange colored rings correspond to the 0,0,1; 0,1,0, and 1,0,0 reflections in order of increasing ring diameter. These reflections correspond to potential systematic absences and are key in determining whether the principle unit cell axes correspond to pure rotation symmetry or screw symmetry. The 0,0,1 reflection appears to be present. The 0,1,0 is absent. The presence or absence of 1,0,0 is uncertain. The XFEL derived spacings shown for a monoclinic cell would not differ significantly for an orthorhombic cell since the β angle is ~90°. (G) and (H) are zoomed in on the low resolution reflections. The edges of both images correspond to 17Å resolution. The maximum projection was obtained from 119 images.

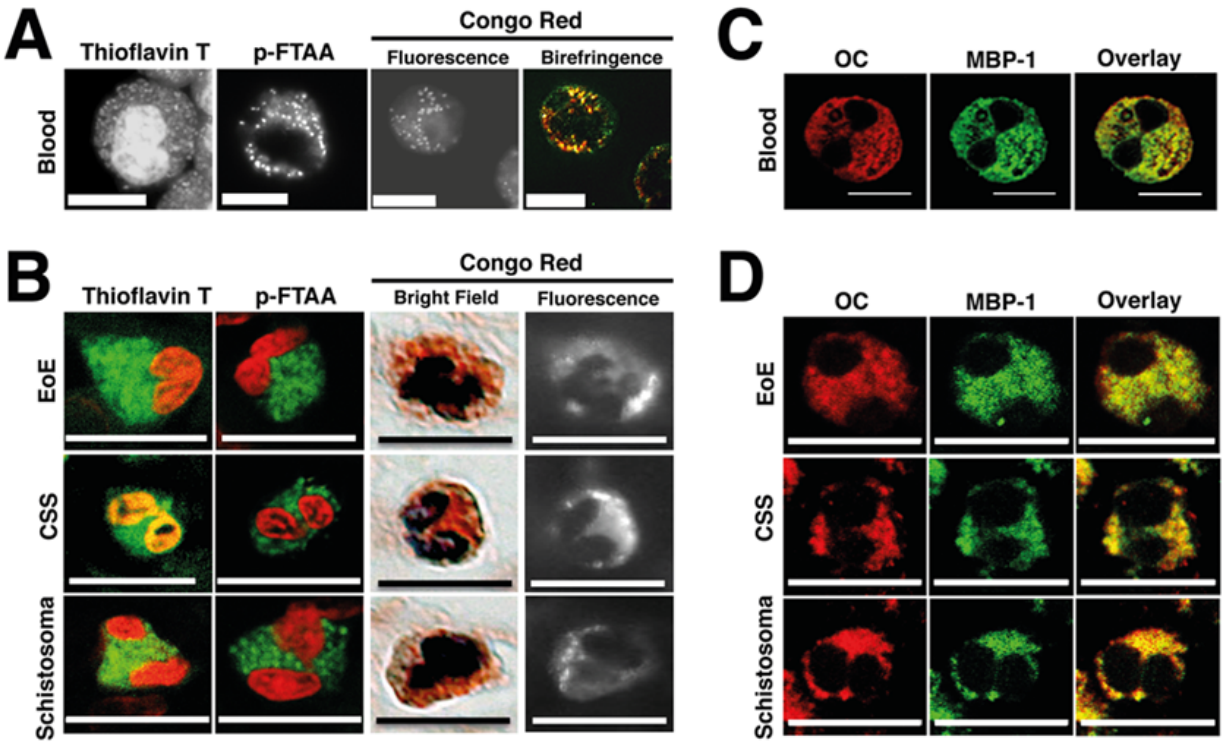

Figure S2. Tinctorial Properties of Eosinophil Granules (related to Fig. 1)
Blood (A) and tissue (B) eosinophils stained with Thioflavin T, p-FTAA and Congo Red. Blood eosinophils could be stained both supravitally as well as after formaldehyde fixation. Tissues were obtained from patients suffering from allergic (eosinophilic esophagitis, EoE; esophagus), autoimmune (Churg-Strauss syndrome, CSS; heart), and infectious diseases (Schistosoma; colon). Nuclei were counterstained with propidium iodide in the Thioflavin T and p-FTAA tissue eosinophil stains. Blood (C) and tissue (D) eosinophils were stained with the OC anti-amyloid aggregates and anti-MBP-1 antibodies. Scale bars: 10 μm.

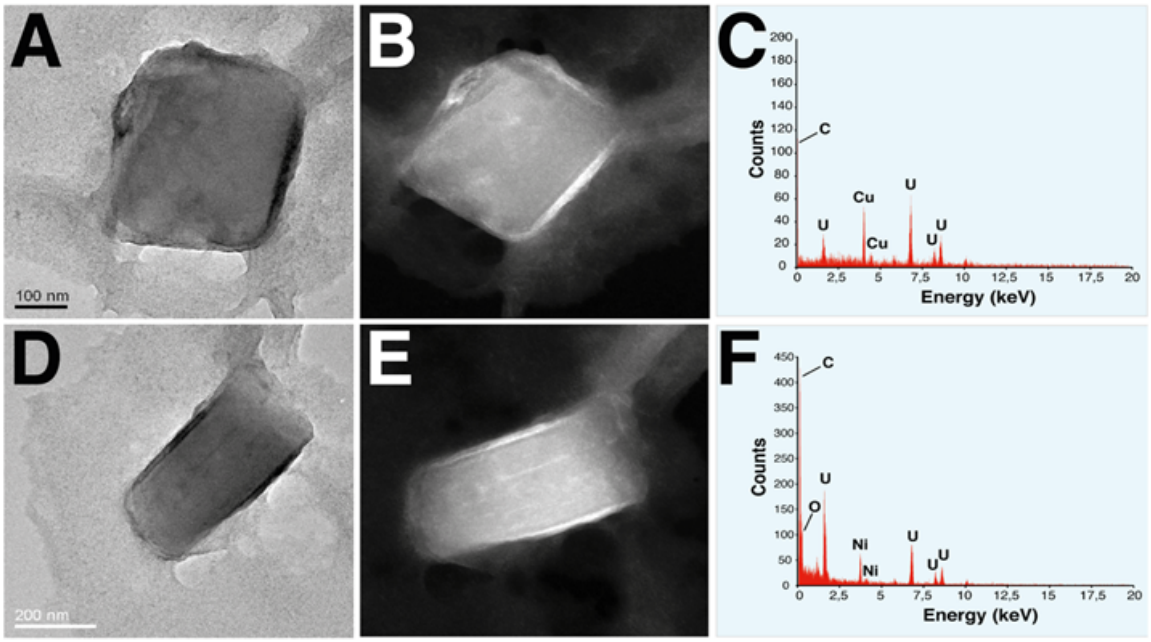

Figure S3. Absence of Heavy Metal Atoms In the Nanocrystalline MBP-1 Cores as Probed by *In Situ* Chemical Analysis (related to Fig. 1)

(A) Negatively stained isolated cores deposited on a carbon coated copper grid examined in bright field mode with a 300 kV TEM microscope. Scale bar: 100 nm.

(B) STEM image of the same core.

(C) STEM-EDX spectrum of the core shows mainly signals arising from the copper grid and the stain.

(D) Cores deposited on a nickel grid visualized in bright field mode. Scale bar: 200 nm.

(E) STEM image of the cores shown in panel D.

(F) The STEM-EDX spectrum shows signals arising from the nickel present in the grid and uranyl acetate from the staining procedure. The signals are labeled by atom type.

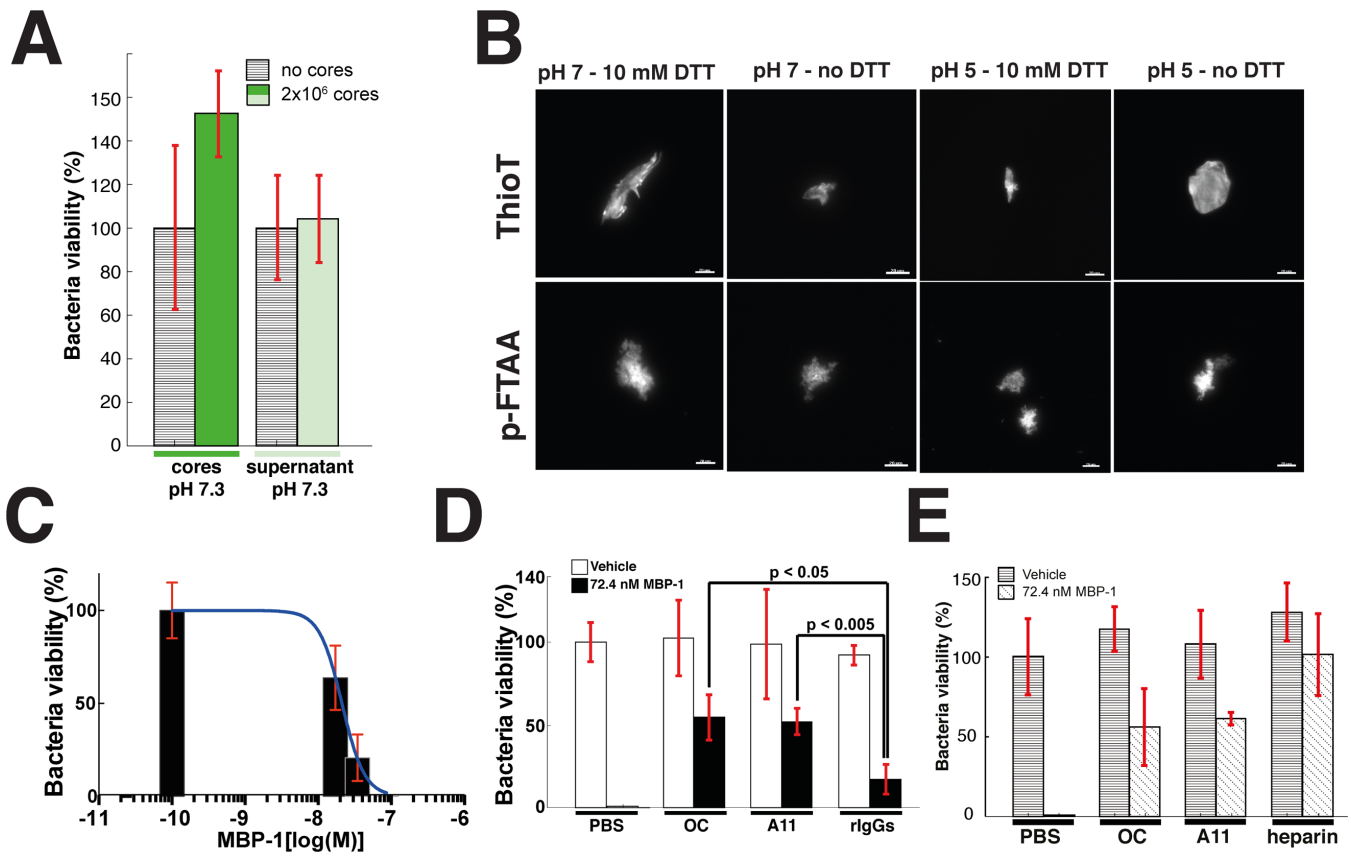

Figure S4. MBP-1 Toxicity Is Reduced by Heparin and Antibodies Specific to Amyloid Aggregates (related to Fig. 2, 3 and 4).

(A) Cores harvested from 2 x 10^6 eosinophils per condition were resuspended in PBS buffer, added to 0.5x10^7 *E. coli*/ml and incubated for 1 h before plating log-dilutions. Neither the entire cores nor the supernatant obtained upon centrifugation of the cores for 20 min at 20'000g exhibited any antibacterial activity.

(B) MBP-1 aggregates stained with the amyloid-specific dyes p-FTAA and Thioflavin T (ThioT). Scale bars: 20 µm.

(C) BKA. Purified MBP-1 was added to *E. coli* at the indicated concentrations. Data are normalized to the buffer control and are presented as mean levels ± % SD (bars) of one representative experiment. The red line represents the nonlinear fit which results in a calculated IC_{50} of ~18 nM.

(D) BKA to quantitate the observations reported in Figure 4A. OC and A11 antibodies significantly inhibited MBP-1 toxicity. Rabbit IgG was used as control.

(E) BKA. Addition of OC and A11 antibodies as well as heparin rescued bacterial viability indicating that interfering with the aggregation process is an effective mean to inhibit MBP-1 toxicity. Mean of three replicates ± % SD are shown.

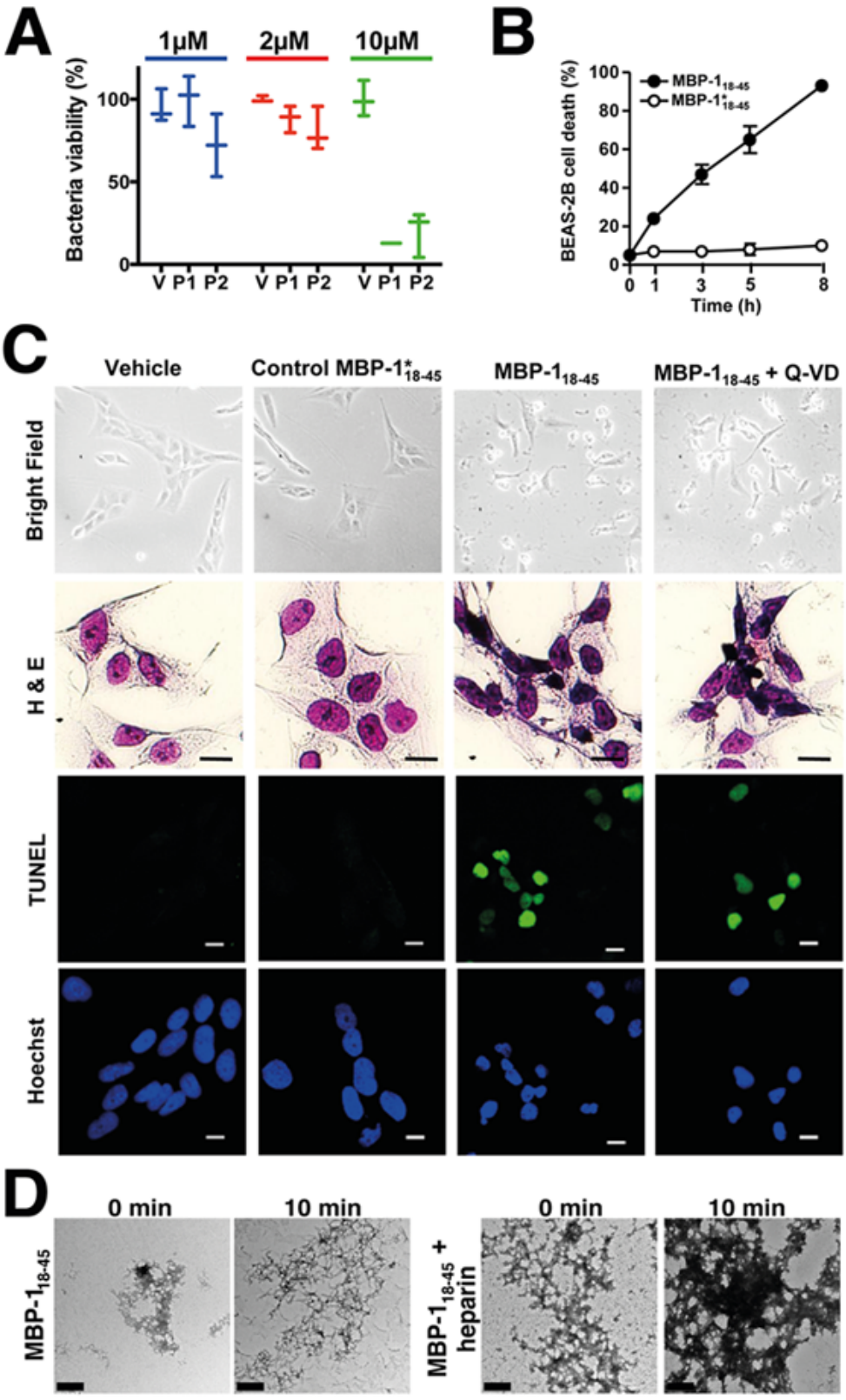
A
1μM
2μM
10μM
Bacteria viability (%)
100
50
0
V P1 P2 V P1 P2 V P1 P2
B
BEAS-2B cell death (%)
MBP-1 18-45
MBP-1* 18-45
100
80
60
40
20
0
0 1 3 5 8
Time (h)
C
Vehicle
Control MBP-1* 18-45
MBP-1 18-45
MBP-1 18-45 + Q-VD
Bright Field
H & E
TUNEL
Hoechst
D
0 min
10 min
0 min
10 min
MBP-1 18-45
MBP-1 18-45 + heparin

Figure S5. MBP-1 Peptide Toxicity Against Bacteria and Human Bronchial Epithelial BEAS-2B Cells (related to Fig. 4)

(A) BKA performed at three different concentrations of MBP-1_{18-45}: 1, 2 and 10 μM. Results for two different peptide batches are shown (P1, P2), while V indicates vehicle treatment (DMSO). Each peptide concentration value was normalized to the corresponding DMSO control. Median values for three replicates ± SEM are shown.

(B) Bronchial epithelial BEAS-2B cells were cultured with 5 μM MBP-1_{18-45} and control peptide for 5 h and analyzed in a time-dependent manner. Data are presented as mean levels ± SD of at least five independent experiments.

(C) Bronchial epithelial BEAS-2B cells were cultured with 5 μM MBP-1_{18-45} or control peptide for 5 h in the presence or absence of the apoptosis inhibitor Q-VD. The MBP-1 peptide induced a relatively round cell shape, loss of cell volume, and detachment as determined by bright field microscopy. Following H&E staining, nuclear condensation was additionally observed. The TUNEL assay indicated that the MBP-1 peptide induced DNA fragmentation, and Hoechst staining provided evidence for both nuclear condensation and nuclear fragmentation. The pharmacological inhibition of caspases, however, did not prevent the MBP-1-induced phenomena. All data are representative of three independent experiments. Scale bars: 10 μm.

(D) TEM of MBP-1_{18-45} aggregates obtained in the presence or absence of heparin. The effect of heparin on inactivation of toxicity can be mediated by the rapid aggregation process which converts toxic species into more inert fibrils.

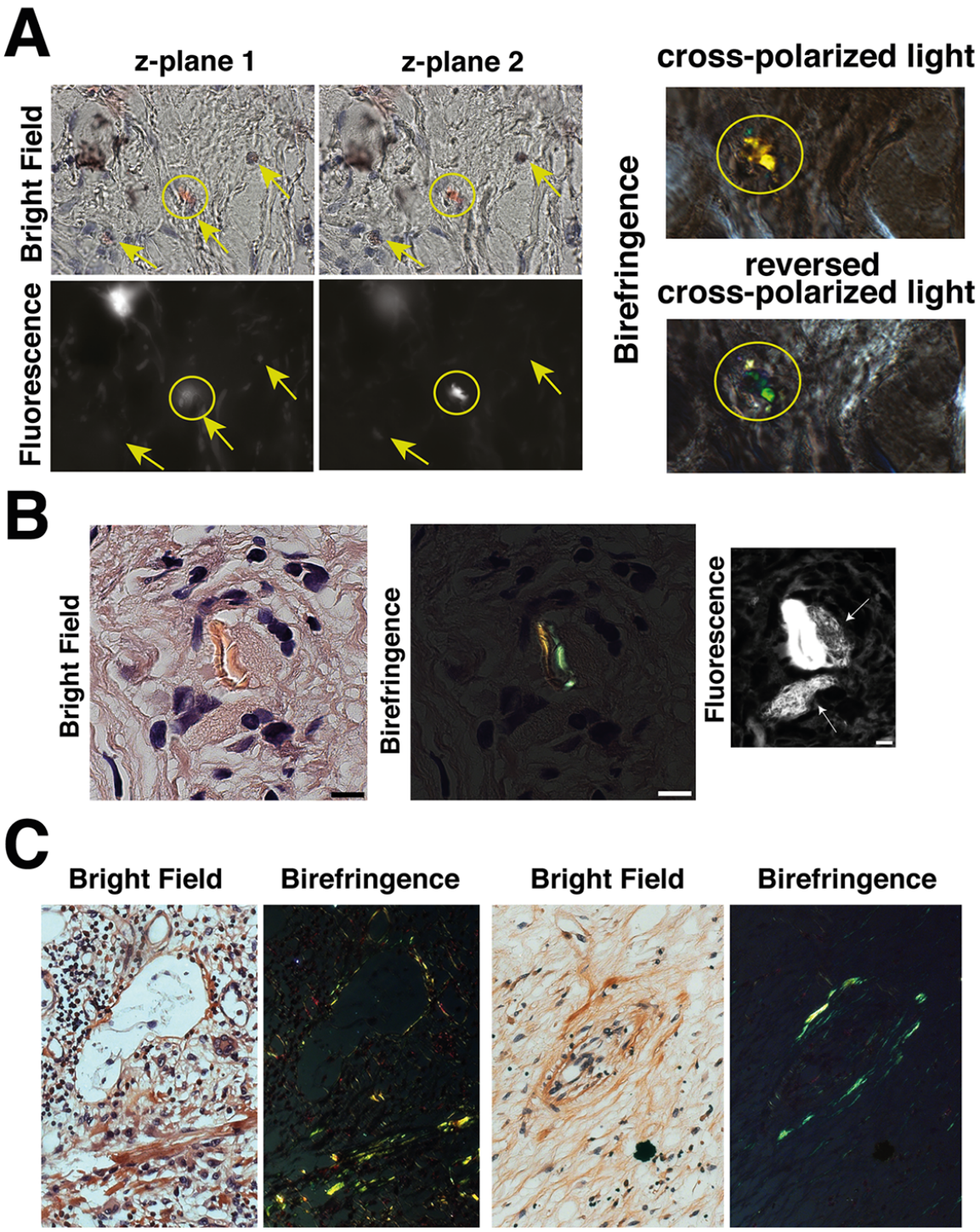
A
z-plane 1
z-plane 2
Bright Field
Fluorescence
cross-polarized light
Birefringence
reversed
cross-polarized light
B
Bright Field
Birefringence
Fluorescence
C
Bright Field
Birefringence
Bright Field
Birefringence

Figure S6. CR Stain of Tissue Biopsies of Patients With Eosinophil Related Diseases (related to Fig. 5)

(A) CR stain of skin tissue from an additional Wells' syndrome patient.
In the bright field and fluorescence mode it is possible to identify several eosinophils (arrows). An eosinophil is justapoxed to an amyloid deposit. This is evident changing the plane from z-plane 1, where the eosinophil is visible, to z-plane 2, where the amyloids are found. If the deposit is observed with cross-polarizers, the amyloid apple-green birefringence is evident. A yellow circle highlights the eosinophil and the extracellular deposit. The birefingent image is zoomed in to display the morphology of the amyloid plaque and confirms its extracellular nature.
(B) CR stain of skin tissue from an atopic dermatitis (AD) patient. Bright field and cross-polarized light images show positive apple green birefringent deposits surrounded by eosinophils. The birefringence is indicative of the presence of ordered amyloid fibrils. The CR fluorescence (right images) shows the presence of more amyloids deposited than visible with birefringence (additional regions highlighted by arrows). Scale bars are 10 μm for the bright field and polarized light images and and 5 μm for the fluorescence picture.
(C) CR stain of heart tissue from a Churg-Strauss Syndrome (CSS) patient.A post mortem evaluation of heart tissue shows extensive amyloid deposition visible as pale-red stained material in bright field mode and apple-green birefringent deposits under cross-polarized light. Magnification: 20x.

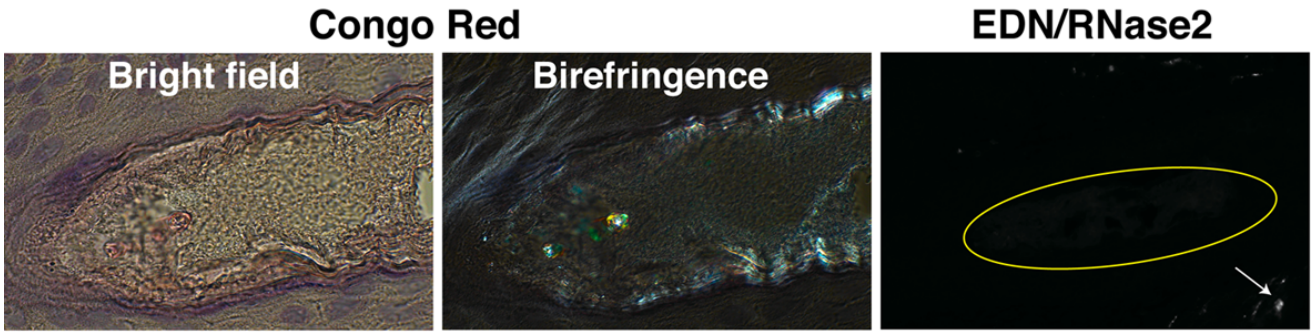

Figure S7. Wells' Syndrome Patient Exhibits Amyloid Deposition in Serial Sections of a Skin Biopsy (related to Fig. 5)

Congo Red stain of skin tissue from a serial section derived from the same sample as Figure 5. Amyloid deposits are stained red and exhibit apple green birefringence under cross-polarized light. These amyloid deposits are not constituted by EDN/RNase2 protein, as visible by the absence of EDN stain on the right, but contain MBP-1 protein (see Figure 5). The area containing the CR-positive amyloid deposit is indicated by a yellow circle while a positively EDN-stained eosinophil is indicated by an arrow. Magnification: 40x.

SUPPLEMENTAL TABLES

Table S1. Experimental Parameters for the XFEL Experiments Performed at LCLS CXI (related to Fig.1).

	LCLS CXI
X-ray focus (nm)	100 - 300
Wavelength (Å)	1.4674
Pulse energy (mJ)	1.125
Fluence at sample (ph*pulse)[a]	8.321×10^{11}
Dose (Ggy/crystal)[a]	2.0
Dose rate (Mgy/fs)[a]	33.3
Exposure time (s)	5×10^{-16}
Detector distance (mm)	230
Temperature (°C)	20
Pressure (torr)	10^{-5}
Shortest shot-to-shot distance (μm)	200[b]
Collection rate (frames/s)	0.2
Hit rate (%)	5.3

[a]Considering a 500x500x500 nm crystal
[b]Indicates only one shot per 200 x 200 μm window

Table S2. Unit Cell Parameters Predicted for Best Diffraction Patterns (related to Fig. 1)

Image	a	b	c	Reflections[a]
r0426_053622	26.636	54.760	58.214	146
r0425_053905	26.846	52.807	59.080	79
r0437_075428	25.765	53.175	59.024	84
r0437_080406	26.280	54.357	59.182	82
Average	26.382 +/- 0.473	53.775 +/- 0.932	58.875 +/- 0.445	

[a]Indicates the number of reflections indexed with I/sigma greater than 1.0

SUPPLEMENTAL EXPERIMENTAL PROCEDURES

Peptide Preparation and Crystallization

Peptide GNLVS (residues 26-30) was synthesized at greater than 97% purity (CS Bio, Menlo Park, CA) and dissolved in water at 20 mg/ml. Crystals were grown at 18°C via hanging-drop vapor diffusion in the presence of 0.1 M phosphate-citrate buffer at pH 4.2 and 2 M ammonium sulfate.

Data Collection and Structure Refinement

Crystals of segment GNLVS were mounted on the ends of pulled glass capillaries. Data was collected at 100 K using a microfocus beam (5x5 μm^2) at the 24-ID-E beamline of the Advanced Photon Source (APS) at Argonne National Laboratory. Data indexing, integration and scaling were performed using XDS/XSCALE (Kabsch, 1993) and DENZO/SCALEPACK (Otwinowski and Minor, 1997). The merged scaled data was imported into the CCP4 format by the programs organized under the "CCP4i" interface (Collaborative Computational Project, 1994). The molecular replacement solution for the segment was obtained using the program PHASER (Read, 2001), using a GAAVA beta-strand sequence as the search model (Murshudov et al., 1997). Crystallographic refinement was performed using PHENIX (Adams et al., 2010). Model building was done with COOT (Emsley and Cowtan, 2004) and illustrated with PYMOL (Delano, 2002).

MBP-1 Purification

Eosinophils were resuspended in 0.25 M sucrose with 250 U/ml of heparin and frozen until needed. Granules were extracted as described in the main text and directly used for protein purification. The proteins were extracted from the granules with 0.01 M HCl (Ohnuki et al., 2005). A Superdex 200 10/300 was equilibrated in 20 mM sodium acetate buffer with 150 mM NaCl at pH 4.2 and the protein mixture derived from the granules was injected at a flow rate of 0.5 ml/min.

The different peaks were run on a denaturing SDS-page gel and MBP-1 was identified from its apparent molecular weight as eluting at 1.4-column volumes, probably due to the strong interaction of the positively charged protein with the column resin. We additionally confirmed its identity by dot blot using an anti-MBP-1 antibody (BMK-13; ab48372, Abcam) and anti-mouse HRP-conjugated secondary antibody (Jackson ImmunoResearch).

Stain with Dyes

MBP-1 aggregates were deposited on a poly-lysine slide (Sigma). For the Thioflavin T staining, a drop of Thioflavin T solution (Sigma) (0.1-1 mM) was added directly on the slide and incubated for 1-2 min, then coverslipped and examined. For the p-FTAA staining, a drop of a 1:100 to 1:1000 p-FTAA dilution at a starting concentration of 1 mg/ml (courtesy of Dr. Andreas Åslund and Dr. Peter Nilsson, IFM, Linköping University, Linköping, Sweden) was added. Images were acquired using an epifluorescent Zeiss 200M (inverse) using the filters GFP-like Ex 485/20, Em 525/30 or TexasRed-like Ex 560/25, Em 607/36. The same protocols were followed for freshly isolated blood eosinophils and paraformaldehyde-fixed eosinophils. For the CR staining, a drop of CR solution from the HT60 kit (Sigma) was added to freshly isolated and formaldehyde-fixed eosinophils, incubated for 2 min, coverslipped and imaged with a Zeiss 200M equipped with double polarizing lenses.

The Thioflavin T, p-FTAA, and CR staining was also performed on 5-μm paraformaldehyde-fixed and paraffin-embedded tissue sections from patients with eosinophilic esophagitis (EoE; esophagus), Churg-Strauss syndrome (CSS; heart), and *Schistosoma* infection (colon). Thioflavin T and p-FTAA staining was performed as previously described (Sigurdson et al., 2007; Maji et al., 2009) and the fluorescence recorded with a laser-scanning confocal microscope (LSM 510, Carl Zeiss Microimaging). CR staining was performed using the HT60 kit according to manufacturer's instructions (Sigma) and images of stained tissues were acquired with a Zeiss 200M microscope.

MBP_{18-45} treatment of cells

20,000 cells were seeded on sterile glass coverslips in a 24-well tissue culture plate and allowed to adhere overnight. Next day, the medium was removed and cells were washed gently three times using DMEM containing 17 mM HEPES (pH 7.2-7.5), but no FBS. The peptides were then added to the cells and incubated for 5 h before fixation in 4% formaldehyde in PBS (pH 7.4), followed by washing three times in PBS. Staining was performed with Hoechst 33342 dye (1 µg/ml; Molecular Probes) for 5 min at room temperature after which the samples were washed three times with PBS, mounted on glass slides using Pro-Gold Mounting Medium (Life Biosciences), and visualized by confocal laser microscopy (LSM 510 Exciter, Carl Zeiss).

Viability Detection

Cell viability was measured after exposure to MBP-1 peptide or control peptide by means of ethidium bromide (1 µM) uptake and flow cytometry (FACS Calibur; BD Biosciences). For morphologic analysis, probes were stained with Diff-Quik dyes and analyzed with an Axiovert 35 microscope equipped with a 63x/numerical aperture 1.4, oil objective lens (Carl Zeiss, Jena, Germany).

Histologic Examination

5-µm tissue sections of human and mouse skin were stained with Hematoxylin & Eosin (H&E) and examined by light microscopy (Axiovert 35; Carl Zeiss).

SUPPLEMENTAL REFERENCES

Adams, P. D. *et al.* (2010). PHENIX: a comprehensive Python-based system for macromolecular structure solution. Acta Crystallogr. D Biol. Crystallogr. *66,* 213–221.

Collaborative Computational Project, Number 4. (1994). The CCP4 suite: programs for protein crystallography. Acta Crystallogr. D Biol. Crystallogr. *50,* 760–763.

Delano, W. (2002). The PyMOL Molecular Graphics System: http://www.pymol.org

Emsley, P., and Cowtan, K. (2004). Coot: model-building tools for molecular graphics. Acta Crystallogr. D Biol. Crystallogr. *60,* 2126–2132.

Kabsch, W. (1993). Automatic processing of rotation diffraction data from crystals of initially unknown symmetry and cell constants. J. Appl. Crystallogr. *26,* 795–800.

Maji, S. K. *et al.* (2009). Functional amyloids as natural storage of peptide hormones in pituitary secretory granules. Science *325,* 328-332.

Murshudov, G. N., Vagin, A. A., and Dodson, E. J. (1997). Refinement of macromolecular structures by the maximum-likelihood method. Acta Crystallogr. D Biol. Crystallogr. *53,* 240–255.

Ohnuki, L.E. *et al*. (2005). Differential extraction of eosinophil granule proteins. J. Immunol. Meth. *307,* 54-61.

Otwinowski, Z., and Minor, W. in *Methods Enzymol.* (Charles W., Carter, J.) Volume *276*, p. 307–326 (Academic Press, 1997).

Read, R. J. (2001). Pushing the boundaries of molecular replacement with maximum likelihood. Acta Crystallogr. D Biol. Crystallogr. *57,* 1373–1382.

Sigurdson, C. J. *et al*. (2007). Prion strain discrimination using luminescent conjugated polymers. Nat. Methods *4*, 1023–1030.